Multimodal Deformable Registration of Traumatic Brain Injury MR Volumes via the Bhattacharyya Distance

Yifei Lou*, Andrei Irimia, Patricio A. Vela, Micah C. Chambers, John D. Van Horn, Paul M. Vespa, and Allen R. Tannenbaum, *Fellow, IEEE*

***Abstract*—An important problem of neuroimaging data analysis for traumatic brain injury (TBI) is the task of coregistering MR volumes acquired using distinct sequences in the presence of widely variable pixel movements which are due to the presence and evolution of pathology. We are motivated by this problem to design a numerically stable registration algorithm which handles large deformations. To this end, we propose a new measure of probability distributions based on the Bhattacharyya distance, which is more stable than the widely used mutual information due to better behavior of the square root function than the logarithm at zero. Robustness is illustrated on two TBI patient datasets, each containing 12 MR modalities. We implement our method on graphics processing units (GPU) so as to meet the clinical requirement of time-efficient processing of TBI data. We find that 6 sare required to register a pair of volumes with matrix sizes of $256 \times 256 \times 60$ on the GPU. In addition to exceptional time efficiency via its GPU implementation, this methodology provides a clinically informative method for the mapping and evaluation of anatomical changes in TBI.**

***Index Terms*—Bhattacharyya distance (BD), deformable image registration, multimodal registration, mutual information(MI), traumatic brain injury (TBI).**

Manuscript received August 10, 2012; revised February 18, 2013; accepted April 13, 2013. Date of publication April 23, 2013; date of current version August 16, 2013. This work was supported in part by the National Center for Research Resources under Grant P41-RR-013218, in part by the National Institute of Biomedical Imaging and Bioengineering under Grant P41-EB-015902 of the National Institutes of Health (NIH), in part by the NIH under Grant R01 MH82918 as well as a grant from AFOSR. This work is part of the National Alliance for Medical Image Computing (NAMIC) supported by the National Institutes of Health through the NIH Roadmap for Medical Research under Grant U54 EB005149. The work of J. D. V. Horn was supported by the NIH through STTR under Grant R41 NS081792. Information on the National Centers for Biomedical Computing can be obtained from http://nihroadmap.nih.gov/bioinformatics. *Asterisk indicates corresponding author.*

*Y. Lou is with the School of Electrical and Computer Engineering, Georgia Institute of Technology, Atlanta, GA 30332 USA (e-mail: louyifei@gmail.com).

A. Irimia, M. C. Chambers, and J. D. Van Horn are with the Laboratory of Neuro Imaging, Department of Neurology, University of California, Los Angeles, CA 90095 USA (e-mail: andrei.irimia@loni.ucla.edu; micahcc@ucla.edu; jack.vanhorn@loni.ucla.edu).

P. A. Vela is with the School of Electrical and Computer Engineering, Georgia Institute of Technology, Atlanta, GA30332 USA (e-mail: pvela@ece.gatech.edu).

P. M. Vespa is with the Brain Injury Research Center, Department of Neurology and Neurosurgery, University of California, Los Angeles, CA 90095 USA (e-mail: pvespa@mednet.ucla.edu).

A. R. Tannenbaum is with the Departments of Electrical and Computer and Biomedical Engineering, Boston University, Boston, MA 02215 USA (e-mail: tannenba@bu.edu).

Color versions of one or more of the figures in this paper are available online at http://ieeexplore.ieee.org.

Digital Object Identifier 10.1109/TBME.2013.2259625

I. Introduction

An estimated 1.7 million Americans sustain traumatic brain injuries (TBI's) every year [1]. The large number of recent TBI cases in soldiers returning from military conflicts has highlighted the critical need for improvement of TBI care and treatment, and has drawn sustained attention to the need for improved methodologies of TBI neuroimaging data analysis. Neuroimaging of TBI is vital for surgical planning by providing important information for anatomic localization and surgical navigation [2], as well as for monitoring patient case evolution over time. Approximately two days after an acute injury, magnetic resonance imaging (MRI) becomes preferable to computed tomography (CT) for the purpose of lesion characterization, and the use of various MR sequences tailored to capture distinct aspects of TBI pathology provides clinicians with essential complementary information for the assessment of TBI-related anatomical insults and pathophysiology.

Deformable image registration (DIR) plays an essential role in TBI image analysis; its aim is to find a transformation between two image sets such that the transformed image becomes similar to the target image according to some chosen metric or criterion. One difficulty in coregistering TBI datasets is the large amount of possible deformation between MR modalities even within the same patient and time point. When it comes to dealing with such large deformations, numerical stability is a critical requirement for registration algorithms. We are motivated by this prominent difficulty of TBI image analysis to propose a novel, numerically stable metric for multimodal image registration.

Multimodal image registration has been an active research area since the seminal work of [3], [4] and, independently, of [5]. When approaching the problem of registering images acquired using distinct MR sequence types, using sum-of-squared-differences of intensity values between two images as a metric of dissimilarity is not useful because tissue types have different intensity profiles from modality to modality. Consequently, the standard strategy for multimodal registration involves comparing intensity distributions instead of intensity values directly. Mutual information (MI) is widely used for this purpose: see the survey in [6] and other more recent work [7]–[10].

MI is a measure which quantifies the mutual dependence of two random variables. Let $p_1(x)$ and $p_2(y)$ be the probability density functions (PDF) of two random variables X and Y, respectively, and let $p(x, y)$ be their joint probability distribution

function. The MI of X and Y is defined as

$$\mathcal{M}(X,Y) = \int_Y \int_X p(x,y) \log \frac{p(x,y)}{p_1(x)p_2(y)} \mathrm{d}x\mathrm{d}y \ . \quad (1)$$

It can also be expressed as a Kullback–Leibler (KL) divergence [11]. Although MI is well defined, its gradient is not, which makes DIR algorithms unstable in the sense that stable algorithms avoid magnifying small errors.

Aside from MI, there are a number of measures in the probability theory which can be used to define a distance between two distributions. Consider the Chi-squared (CS) statistic [12], for example. It is defined as

$$\chi^2 = \sum_i \frac{(X_i - Y_i)^2}{X_i + Y_i} \quad (2)$$

where X_i and Y_i are the frequency-coded quantities contained in bin i for X and Y, respectively. The main drawback of this measure is that singularities arise when computing the CS for empty bins.

This paper explores the possibility of avoiding the potential instability problems of MI and CS by using the Bhattacharyya distance (BD) [13] for the problem of multimodal DIR. It should be noted that the BD is similar to the Jensen–Renyi divergence [14] and identical to the I_α information with $\alpha = 0.5$ in [15]; nevertheless, neither of these measures has been sufficiently studied from the standpoint of their possible relevance to the problem of image registration. Our main purpose in this paper is to propose a stable information-theoretic metric as an alternative to CS and MI, which are currently standard in medical imaging registration. [16], for example, illustrates some advantages of BD over CS, such as the former being "self consistent, unbiased, and applicable to any distribution." Similarly, [17] notes that the BD leads to better results than the KL divergence in signal selection, which implies that the BD may be better than MI for the problem of DIR. Recently, the BD has shown its potential in various applications to computer vision, such as detection [18], segmentation [19], and tracking [20], [21].

In clinical settings, which involve acute TBI care, the amount of time required for the processing of neuroimaging datasets from patients in critical condition should be minimized. To meet this clinical requirement, we implement our algorithm on a graphics processing unit (GPU) platform. The robustness of the method is illustrated using two sample TBI patient datasets, each containing 12 pairs of multimodal MR volumes at both acute and chronic stages. We also provide a clinically informative way to map and evaluate anatomical changes in TBI.

The unusual heterogeneity of TBI and large variability of pathology-related tissue intensities across modalities are two appreciable difficulties which must be considered when evaluating registration methods designed specifically for TBI. These two factors make our validation task significantly more challenging than that involving registration methods for healthy MR data, where more subjects are typically used than in our case. Although our validation approach is admittedly limited and illustrative at least due to the use of only two subjects, our results do provide an adequate−though preliminary−basis for evaluating the benefits of our proposed method.

The remainder of this paper is organized as follows. Section II derives the formula of the similarity measures based on the BD. A viscous fluid model is reviewed in Section III as a registration framework to compare MI to the BD. In Section IV, we conduct a quantitative and qualitative analysis on two synthetic sets of data including phantoms, simulated MRIs; subsequently, two authentic TBI patient datasets are examined separately in Section V. Finally, conclusions and directions for future research are given in Section VI.

II. Theoretical Framework

The formula of the similarity measure via the Bhattacharyya coefficient (BC) is derived in the same way in which MI can be derived from the KL divergence. Since both the BD and MI stem from the use of a divergence measure, both measures are similarly able to distinguish between two distributions. The BD is advocated here as a similarity measure for the problem of DIR due to the fact that the gradient of MI is not well defined, which leads to instability in the iterative process for approaching optimal solutions.

The KL divergence is a nonsymmetric measure of the difference between two probability distributions P and Q, defined as

$$\mathcal{D}_{\mathrm{KL}}(P,Q) = \int p(r) \log \frac{p(r)}{q(r)} \mathrm{d}r \quad (3)$$

where p and q are the PDFs of P and Q. Then, MI (1) can be interpreted in terms of the KL divergence of the product $p_1(x) \times p_2(y)$ and the joint distribution $p(x,y)$:

$$\mathcal{M}(X,Y) = \mathcal{D}_{\mathrm{KL}}(p(x,y), p_1(x)p_2(y)) \ . \quad (4)$$

On the other hand, the BD [13] defines a symmetric distance between probability distributions as $-\log \mathcal{D}_{\mathrm{BC}}$, where $\mathcal{D}_{\mathrm{BC}}$ is the BC, given by

$$\mathcal{D}_{\mathrm{BC}}(P,Q) = \int \sqrt{p(r)q(r)} \mathrm{d}r \ . \quad (5)$$

Replacing the KL divergence in (4) with the BC, one obtains the expression for a similarity metric

$$\mathcal{B}(X,Y) = \mathcal{D}_{\mathrm{BC}}(p(x,y), p_1(x)p_2(y)) \quad (6)$$

$$= \int \sqrt{p(x,y)p_1(x)p_2(y)} \mathrm{d}x\mathrm{d}y \ . \quad (7)$$

Similarly to MI, this metric can be used in registering two images with different modalities, since both of them illustrate some type of divergence between two distributions $p(x,y)$ and $p_1(x)p_2(y)$. Hence forward, the convention is adopted of expressing $\mathcal{B}(X,Y)$ in (7) using the BD, as opposed to MI.

For DIR, one is interested in computing the displacement field $T(\vec{z}) = z - \vec{u}(\vec{z})$ which deforms one image I_1, often called the *moving* image, to match the *static* image I_2 by mapping the fixed position $\vec{z}$ in I_2 onto the corresponding point $\vec{z} - \vec{u}$ in I_1. The optimal solution of $\vec{u}$, which is often called a deformation field, is obtained by maximizing MI or by minimizing the BD between two PDFs of $I_1(\vec{z} - \vec{u})$ and $I_2(\vec{z})$. The PDF is expressed in terms of the intensity histogram. Consider, for example, the joint intensity distribution (or, for short, the joint histogram)

in this scenario, which can be computed using a 2-D Parzen window

$$G_\sigma(a,b) = \exp\left(-\frac{a^2+b^2}{2\sigma^2}\right) \tag{8}$$

to approximate the δ function in the overlap region V:

$$\begin{aligned} p(i_1,i_2;\vec{u}) &= \frac{1}{V}\int_V \delta(i_1 - I_1(\vec{z}-\vec{u}), i_2 - I_2(\vec{z}))\mathrm{d}\vec{z} \\ &\simeq \frac{1}{V}\int_V G_\sigma(i_1 - I_1(\vec{z}-\vec{u}), i_2 - I_2(\vec{z}))\mathrm{d}\vec{z}\,. \end{aligned} \tag{9}$$

Its marginal distributions $p(i_1;\vec{u}), p(i_2)$ are the PDFs of $I_1(\vec{z}-\vec{u})$ and $I_2(\vec{z})$, respectively. To simplify notation, it is assumed that the BD and MI are directly defined on images

$$\mathcal{B}(I_1,I_2;\vec{u}) = \iint \sqrt{p(i_1,i_2;\vec{u})p(i_1;\vec{u})p(i_2)}\mathrm{d}i_1\mathrm{d}i_2 \tag{10}$$

$$\mathcal{M}(I_1,I_2;\vec{u}) = \iint p(i_1,i_2;\vec{u})\log\frac{p(i_1,i_2;\vec{u})}{p(i_1;\vec{u})p(i_2)}\mathrm{d}i_1\mathrm{d}i_2\,. \tag{11}$$

It is standard to obtain the optimal solution of the deformation $\vec{u}$ via an iterative gradient descent algorithm. The gradients of the BD and MI with respect to $\vec{u}$ share the same structure

$$\frac{1}{V}\left[\frac{\partial G_\sigma}{\partial i_1}L(i_1,i_2,\vec{u})\right](I_1(\vec{z}-\vec{u}), I_2(\vec{z}))\nabla I_1(\vec{z}-\vec{u}) \tag{12}$$

where the L term for the BD and MI is given by

$$L_B(i_1,i_2;\vec{u}) = \frac{1}{2}\sqrt{\frac{p(i_1;\vec{u})p(i_2)}{p(i_1,i_2;\vec{u})}} + \frac{1}{2}\int\sqrt{\frac{p(i_2)p(i_1,i_2,\vec{u})}{p(i_1;\vec{u})}}\mathrm{d}i_2 \tag{13}$$

$$L_M(i_1,i_2;\vec{u}) = 1 + \log\frac{p(i_1,i_2;\vec{u})}{p(i_1;\vec{u})p(i_2)}. \tag{14}$$

The subscripts B and M correspond to the BD and MI, respectively. The deviation of the MI-based gradient is presented in [22], and is similar to the calculation of the BD-based gradient.

Although the gradient of the MI is much simpler to compute than that of the BD, it has a major drawback stemming from the *logarithm* function involved in its computation. It is well known that the value of the logarithm function is highly sensitive to variations of its argument taking relatively small positive values. Since it is undefined at zero, it results that computing the gradient of MI is prone to numerical errors near the origin. As for the BD, the square root is continuous at zero, thus making it less susceptible to computational errors.

From the standpoint of computational complexity, it seems more expensive to compute the gradient of the BD than that of MI when comparing (13) and (14). However, the difference in the computational cost of the similarity measure does not affect the overall computational time for registration. Since the dimension of the 2-D joint histogram is usually much smaller than the sizes of 3-D images, the additional cost of computing (13) other than (14) is negligible. In other words, the BD has the same computational cost as MI for each iteration in this DIR framework.

III. Viscous Fluid Model for Registration

A registration algorithm is usually composed of three main components: a transformer, a measure, and an optimizer. Typically, a similarity measure is first established to quantify how close two image volumes are to each other according to some chosen metric. Next, the transformation which maximizes this similarity is computed through an optimization process which constrains the transformation to a predetermined class, such as rigid, affine, or deformable. For example, a rigid transformation is parameterized by six degrees of freedom, i.e., translation and rotation. In this study, the focus is upon the local deformation of the brain, which is difficult to describe via parameterized transformations. Consequently, a free-form deformation model is chosen here, where the number of degrees of freedom of $\vec{u}$ is the same as the number of pixels in the image volumes, contrary to the case of B-splines [23], where deformation is defined on a number of control points and where the motion between points is propagated by interpolation. The use of B-splines may result in inaccuracy and may cause artifacts if the grid of control points is coarse. On the other hand, a dense grid fails to handle large deformations as local folding of the deformation is not allowed. In spite of their drawbacks, B-splines are still widely used for DIR with the combination of a multiresolution approach. One important contribution of this paper is that we propose to replace the MI criterion for multimodal registration with the BD, which can be applied to B-spline types of implementations as well.

In the viscous fluid model proposed in [22], the deformation is assumed to be governed by the Navier–Stokes equation of viscous fluid motion, mathematically expressed as

$$\nabla^2\vec{v} + \vec{\nabla}(\vec{\nabla}\cdot\vec{v}) + \vec{F}(\vec{z},\vec{u}) = 0. \tag{15}$$

The deformation velocity $\vec{v}(\vec{z},t)$ is related to $\vec{u}$ by

$$\vec{v} = \frac{\mathrm{d}\vec{u}}{\mathrm{d}t} = J(\vec{u})\vec{v} + \frac{\partial\vec{u}}{\partial t} \tag{16}$$

where $J(\vec{u})$ is the Jacobian of $\vec{u}$. $\vec{F}(\vec{z},\vec{u})$ is the force field which drives the deformation in the appropriate direction. In [22], the purpose of the force is to maximize MI, whereas the innovation here is to use the BD. The force term is parallel to the image gradient of certain similarity measures with respect to the deformation $\vec{u}$. It should be noted that the goal is minimizing the BD as opposed to maximizing MI, and consequently the force in (12) exhibits a *negative* L_B term (13).

To solve the Navier–Stokes equation (15), successive over-relaxation (SOR) may be applied as in [24], although this is computationally expensive. Fourier methods are proposed in [25] to solve this equation efficiently. Alternatively, the approach adopted here involves convolving the force field with the 3-D Gaussian kernel Φ_s as an approximation to the solution [22], [26]. In summary, the deformation field $\vec{u}$ at iteration k is given by

$$\vec{v}^k = \Phi_s\vec{F}^k \tag{17}$$

$$\vec{R} = \vec{v}^k - \sum_{i=1}^{3} v_i^k\left[\frac{\partial u^k}{\partial z_i}\right] \tag{18}$$

$$\vec{u}^{k+1} = \vec{u}^k + \delta_t\vec{R} \tag{19}$$

where $\vec{z} = (z_1, z_2, z_3)^T, \vec{v} = (v_1, v_2, v_3)^T$. The time step δ_t is chosen adaptively during iteration and set to

$$\delta_t = \frac{\delta_u}{\max\|\vec{R}\|} \tag{20}$$

with δ_u (in voxels) being the maximal voxel deformation which is allowed in one iteration. The numerical errors involved in computing the gradient of MI can cause large gradient values, i.e., $\max\|\vec{R}\|$ can be large. It follows from (20) that one should use a smaller δ_t in order to make the iterative algorithm more stable. Consequently, the MI formulation needs more iterations to converge compared to the BD.

To preserve the topology of the deformed template, regridding is performed when there exists $\vec{z}$ such that the Jacobian of $\vec{z} - \vec{u}$ becomes less than a positive value. As long as the determinant of the Jacobian is larger than this predetermined value, the deformation field is guaranteed to be invertible, and thus the topology is preserved. In [22], this value is chosen to be 0.5, which is also used in our case. Regridding is performed in such a way that the current deformed image is set to a new template, and the incremental deformation field is set to zero. In the end, the total deformation is the concatenation of the incremental deformation fields associated with each propagated template. An alternative strategy to preserve topology is to use topology-preserving geodesics, such as [27]–[29]. However, these methods are computationally expensive.

A. Proposed Algorithm

The gist of our innovation is the replacement of MI by the BD during registration. The viscous fluid approach in [22] is adopted here, although the proposed replacement of MI by the BD can be applied to B-spline implementations as well. In summary, our multimodal DIR algorithm proceeds as follows: at each iteration step k,

1) warp the input image according to the previous deformation field, i.e., $I_1(\vec{z} - \vec{u}^{k-1})$;
2) compute the joint histogram $p(i_1, i_2; \vec{u})$ via (9);
3) compute the marginal histograms by integrating $p(i_1, i_2, \vec{u})$ over rows and columns respectively;
4) update the deformation field $\vec{u}^k$ according to (17)–(19), in which the force term $\vec{F}$ is defined by (12) with the *negative* L_B term (13).
5) regrid if necessary

A multiresolution scheme is employed to increase the speed and robustness. Specifically, the deformation field that is obtained at the lower resolution is fed back at the initial value for the higher resolution. To meet the clinical requirement of drastically reducing processing times, the algorithm is implemented on a GPU, where it takes 6 s to register two image volumes of size $256 \times 256 \times 60$ for 50 iterations using three multiresolution levels. Please refer to [30] for more details on the GPU implementation.

IV. Analysis

Results of volume registration using the BD and MI in the viscous fluid frame are compared here using three different experiments. First, synthetic phantoms are employed to show that MI may not perform as well on images with only a few different intensity values. Second, smooth deformations are manually applied to simulated MR images of human brains. Because the ground truth of the deformation is known, one can thereby assess the accuracy and robustness of the two metrics. Finally, a realistic application is presented by means of coregistering two TBI patient datasets, each contains 12 MR modalities at two clinical stages (acute and chronic).

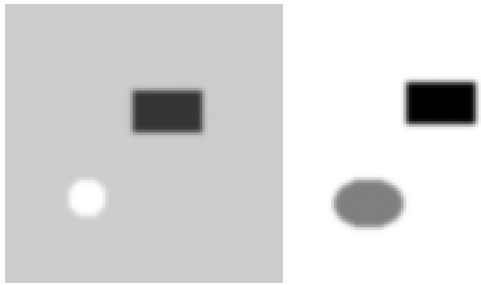

Fig. 1. Toy example: (left) moving image and (right) static image.

Registration results are visualized using a checkerboard display tool. In this technique, the two images to be compared are merged together in a checkerboard pattern where the black region is filled by one image and the white region is filled by another. At the transition zone, this manner of display makes the mismatch between anatomical structures in the two images visible. Ideally, when two images are fully aligned, there is no difference in the boundary between checkerboard squares.

A. Synthetic 2-D Images

The moving image is synthesized by smoothing a three-value image with difference intensities on the rectangle, the circle, and the background. Similarly, the static image has the rectangle moving down left and the circle expanding to an ellipse. Fig. 1 shows these two test images for multimodal registration. In this case, the majority values in the joint histogram are zero, thus yielding instability in the MI-based approach. With the same number of iterations, MI does not completely match the circle to the ellipse, nor does it move the rectangle, whereas the BD is successful on both regions as shown in the checkerboard comparison in Fig. 2. With more iterations, MI is able to match the ellipse, but it still fails to move the rectangle. This illustrates that MI converges more slowly than the BD. This example clearly demonstrates that MI is not as good as the BD in such a registration scenario, and the reasons are three-fold. First, MI is not as accurate as the BD (the concept of accuracy for a similarity measure is examined more carefully in Section IV-B.) In fact, one can find a counterexample where the MI of two unmatched rectangles is larger than that of matched ones that is why the MI-based registration method fails to match the rectangles in the two images. Second, the numerical errors introduced by the presence of the logarithm function can cause the gradient of MI to be erroneously large. As a result, a smaller δ_t in (20) has to be chosen to make the algorithm stable, thus yielding a slow convergence. Finally, the gradient of MI is not

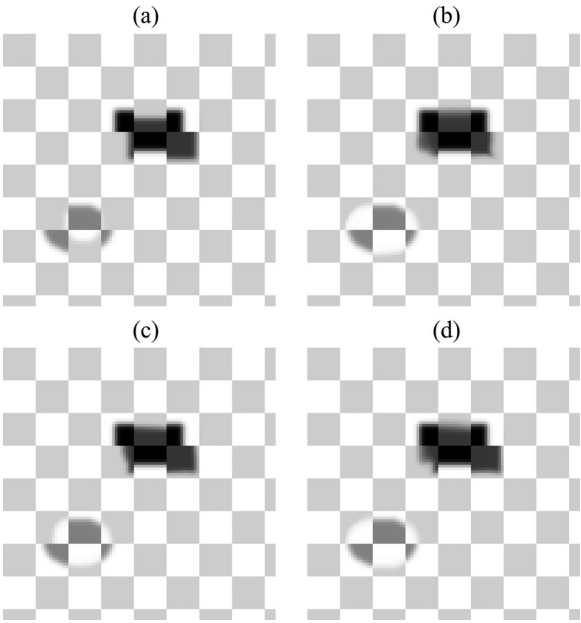

Fig. 2. Checkerboard comparison. (a) original data, (b) BD with 50 iterations, (c) MI with 50 iterations and (d) MI with 100 iterations. MI needs more iterations than BD to completely match the circle to the ellipse and it fails to move the rectangle.

accurate itself either, as the iterative algorithm for it is stuck at a local minimum.

B. Simulations

Simulated MR brain images from the BrainWeb [31] are used in this experiment. Triplets of T_1/T_2/PD images are selected with a slice thickness of 1mm, a noise level 3%, and different intensity nonuniformity levels $(0\%, 20\%, 40\%)$. Fig. 4(a)–(c) shows sample images of T_1, T_2, PD, respectively.

An optimization-independent evaluation of the BD and MI based on the work of [32] is presented here, where five properties for the assessment of a similarity measure are assessed. The most important of these, i.e., accuracy (ACC), which describes the behavior of a similarity measure close to the "gold standard," is selected here and analyzed as follows. First, a set of control points which lie on a 2-D grid of $6\times$ 7 knots with a size of 30 mm are selected. One control point is examined at a time by displacing it in various combinations of random directions and distances from its original position while perturbing all the other control points. Each such displacement generates a local deformation, which can be applied to a (moving) image. The similarity measure is then computed between the deformed image and the fixed one. The position of the control point which yields the optimal similarity measure is compared to the gold standard, i.e., its original position, in terms of ACC. The pseudocode to compute ACC is described in Algorithm 1 with the help of the diagram in Fig. 3. The parameters in Algorithm 1 are set to $R = 20$ mm, $N = 10$, $M = 40$, $RD = 1$mm. Table I lists the means and standard deviations of the ACC of the BD and MI over 20 random realizations, which show that the BD is better than MI in terms of measuring similarity between two images.

Algorithm 1 Pseudo-code to compute ACC

Let SM(X) be the value of a similarity measure. Define the "gold standard" position of one control point as X_0.
for each probing line ($n = 1$ to N) **do**
  Randomly select the direction of the probing line $(X_{n,M/2} - X_{n,-M/2})$.
  Displace all other control points for distance RD with random directions.
  for each point evenly spaced on the probing line ($m = -M/2$ to $M/2$) **do**
    Displace the origin X_0 to the position $X_{n,m}$
    Deform the floating image according to the positions of all control points
    Compute the similarity measure value SM($X_{n,m}$) between the moving and the static image
  end for
end for
Let $X_{n,max}$ be the position of the global maximum of the similarity measure SM($X_{n,m}$) along line n.
The accuracy(ACC) of a similarity measure is defined as

$$ACC = \sqrt{\frac{1}{N}\sum_{n=1}^{N} \|X_{n,max} - X_0\|^2}.$$

Please refer to the diagram in Figure 3 and [32] for more information.

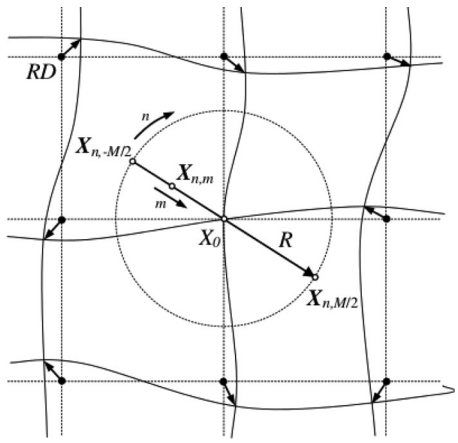

Fig. 3. Figure courtesy to [32]: systematic displacements of one control point X_0 to $X_{n,m}$ and displacements of neighboring control points for a distance RD in random directions.

TABLE I
MEANS AND STANDARD DEVIATIONS (MEASURED IN PIXELS) OF THE ACC FOR THE BD AND MI ARE REPORTED WITH 20 RANDOM REALIZATIONS

Level	T_1/T_2		T_1/PD	
	MI	BD	MI	BD
0%	0.4746(0.12)	**0.4207**(0.17)	0.4479(0.20)	**0.4081**(0.21)
20%	0.5409(0.13)	**0.4620**(0.20)	0.4996(0.16)	**0.4868**(0.17)
40%	0.6693(0.23)	**0.6182**(0.20)	0.6402(0.16)	**0.6348**(0.16)

The BD is slightly better than MI in terms of measuring similarity between the two images.

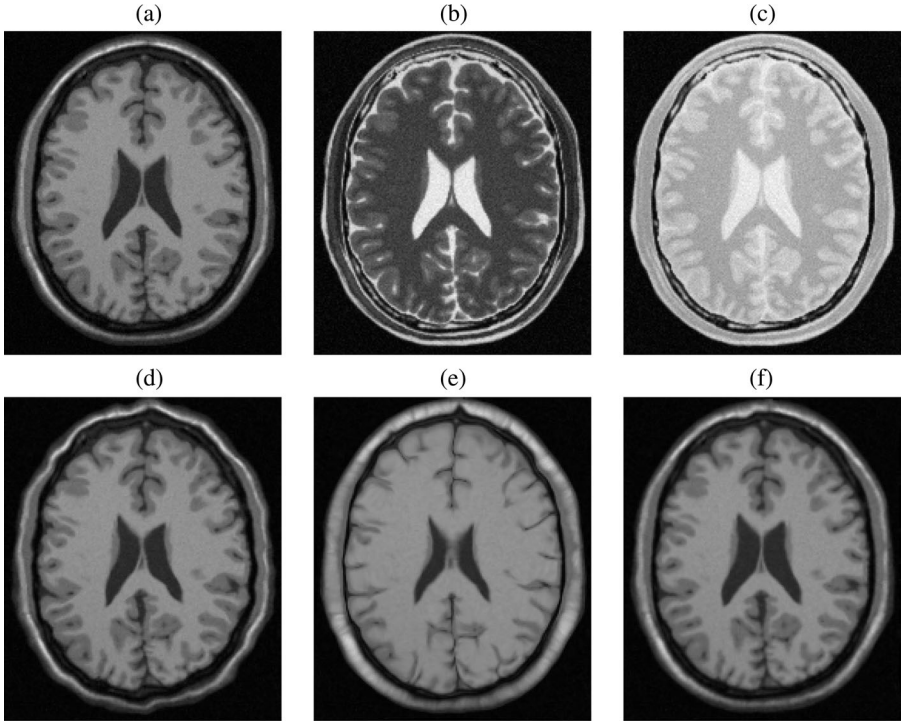

Fig. 4. Registration results on the simulated MRI. (a)–(c) are sample images of T_1, T_2, and PD, respectively. The manually deformed T_1 is shown in (d), which is further deformed to match T_2 by deformable registration using MI and BD. The registration result using MI, shown in (e), is erroneous in that white matter is swollen and gray matter and ventricle are shrunk, while the one using BD, shown in (f), is visually pleasing and looks similar to (a), the original T1. (a) T_1. (b) T_2. (c) PD. (d) Deformed T_1. (e) Registered by MI. (f) Registered by BD.

TABLE II
MEANS AND STANDARD DEVIATIONS (MEASURED IN PIXEL) OF RMS OF BD AND MI ARE REPORTED WITH 20 RANDOM REALIZATIONS

Level	T_1/T_2		T_1/PD	
	MI	BD	MI	BD
0%	1.1187(0.14)	**0.95**(0.04)	1.3603(0.15)	**0.9445**(0.04)
20%	1.5978(0.15)	**0.9442**(0.03)	1.2595(0.17)	**0.9439**(0.03)
40%	1.0005(0.04)	**0.9348**(0.04)	1.7248(0.15)	**0.9474**(0.03)

BD outperforms MI when the viscous fluid model is applied to obtain the optimal solution.

In other words, the BD is a more accurate similarity measure compared to MI, independent of the optimization scheme to construct the deformation field.

To conduct a quantitative comparison of registration accuracy between MI and the BD when taking into account the optimization algorithm, one 2-D slice of a T_1 image is artificially deformed according to a random deformation. To make the deformation realistic, it is smoothed by a Gaussian kernel. Registration is performed by choosing this manually deformed T_1 image as the static image and the same 2-D slice on T_2/PD as the moving image. The computed deformation fields using MI or the BD are compared with the ground truth using the root-mean-square (RMS) measure. Table II shows that the BD outperforms MI when the viscous fluid model is applied to construct the deformation field.

In addition, the deformed T_1 image is deformed back to T_2, so that the output of the registration algorithm looks close to the original T_1 image. The registration result using MI, shown in Fig. 4(e), is erroneous in that white matter is swollen whereas gray matter and the ventricles are shrunk. The instability of MI indicates that a number of regriding steps need to be performed in order to maintain diffeomorphic deformations, in which errors existing in registration and interpolation propagate. The one using the BD, shown in Fig. 4(f), is visually pleasing and looks similar to the original T_1 image.

V. REALISTIC APPLICATION TO TBI VOLUMES

The algorithm developed in this study was validated on two patient sets of multimodal MR volumes, which were acquired at 3 T using a Siemens Trio TIM scanner (Siemens AG, Erlangen, Germany). Because assessing the time evolution of TBI between the acute and chronic stage is of great interest in the clinical field in order to evaluate case evolution, scanning sessions were held both several days (acute baseline) as well as six months (chronic follow-up) after the traumatic injury event. To eliminate the effect of different scanner parameters during each scanning session, every subject was scanned using the same scanner for both acute and chronic time points. The MP-RAGE sequence [33] was used to acquire T_1-weighted images. In addition, MR data were also acquired using fluid-attenuated inversion recovery (FLAIR, [34]), gradient-recalled echo (GRE) T_2-weighted images, diffusion weighted imaging (DWI), and perfusion imaging.

A. Preprocessing

The clinical data presented here are for the same patients scanned at two time points (acute and chronic). All image volumes were coregistered by rigid-body transformation to the

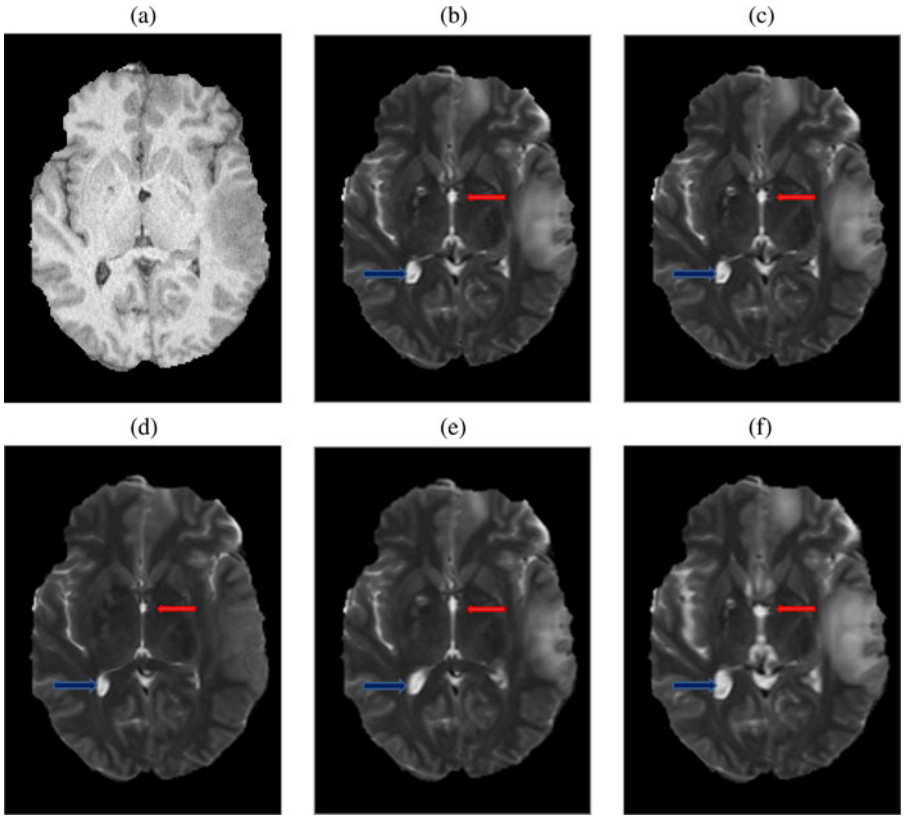

Fig. 5. Registration comparison: deforming T_2 to match T_1. The viscous model based on either MI or the BD is compared with NiftyReg [40] and ANTs [41]. (a) T_1 (static). (b) T_2 (moving). (c) by NiftyReg. (d) by MI. (e) by BD. (f) by ANTs.

precontrast T_1-weighted volume acquired during the acute baseline scanning session with a spatial resolution of 1 mm^3 and a matrix size of 256×256×60. This approach is helpful when accounting for head tilt and when attempting to reduce errors in computing the local deformation fields. Another operation which is applied before performing the registration is skull stripping, which is an important preprocessing step in many neuroimaging analyses [35]–[37]. It is a particularly useful operation in our case because images acquired in some modalities exhibited appreciably more extracranial swelling compared to others; without skull stripping, the registration algorithm would try to match the outer boundary. In addition, having a brain mask decreases the computational time in our case. It should be noted that it is not necessary to have a very accurate brain mask because the brain is the main structure of interest in TBI image analysis. We use BrainSuite software [38] for skull stripping. Because all modalities are coregistered to T_1, one only needs to perform skull stripping once, i.e., on the T_1 volume.

B. Computational Efficiency

The DIR algorithm using both the BD and MI is implemented in C++ and CUDA[1] and executed on a personal laptop with 1.80 GHz CPU and an NVIDIA Tesla C1060 GPU. Both similarity measures are found to require approximately the same amount of time regardless of which platform is used. Furthermore, the parallel GPU implementation achieves speedup by a factor of 50 compared to one serial CPU. The deformable registration of two volumes of sizes 256×256×60 is found to require 6 s. Registration is performed with three multiresolution levels, with a maximum of 50 iterations on each level and with 256 histogram bins.

For comparison, BRAINSFit [39], NiftyReg[2] [40], and ANTs[3] [41] were tested on the same data under identical hardware configurations. All of these methods have the option to use MI as the similarity measure. In addition, BRAINSFit and NiftyReg are both B-spline based implementations, while ANTs implements a diffeomorphic deformation. BRAINSFit is used here as a plugin in 3D Slicer[4], and is found to require 8 min. NiftyReg contains both CPU and GPU implementations of the method [23], which takes 15 min and 35 s (CPU) and 2 min 18 s (GPU). ANTs, a diffeomorphic registration method, requires 1 h and 4 min.

C. Visual Comparison

Figs. 5 and 6 show registration results between T_1 and T_2 of patient #1 and between T_1 and FLAIR of patient #2, respectively. The registered T_2 by NiftyReg looks almost like the original T_2, which implies that the deformation it computes is very small. Similar behavior is observed that the registered FLAIR by BRAINSFit resembles the original FLAIR. In Fig. 5,

[1]CUDA is a software platform for general-purpose programming on GPU.

[2]http://www0.cs.ucl.ac.uk/staff/M.Modat/Marcs_Page/Software.html
[3]http://www.picsl.upenn.edu/ANTS/
[4]http://www.slicer.org

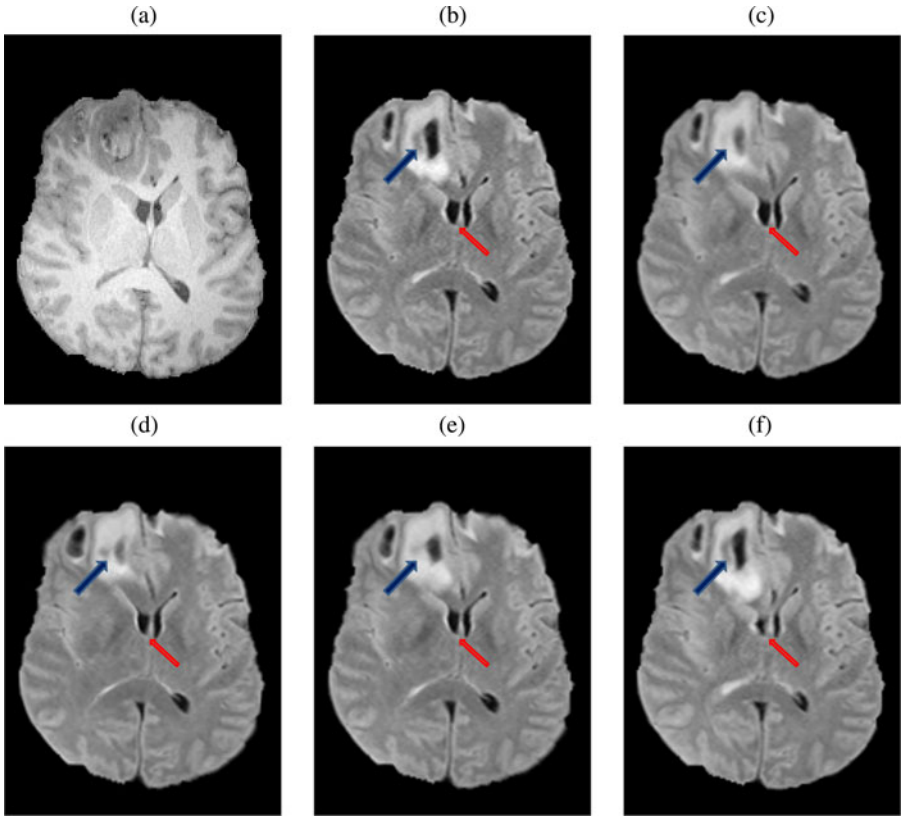

Fig. 6. Registration comparison: deforming FLAIR to match T_1. The viscous model based on either MI or the BD is compared with BRAINSFit [39] and ANTs [41]. (a) T_1 (static). (b) T_2 (moving). (c) by BRAINSFit. (d) by MI. (e) by BD. (f) by ANTs.

the posterior portion of the left lateral ventricle (blue arrow) and part of the third ventricle (red arrow) of ANTs registered image are swollen, while these regions are found to shrink too much in the MI-registered image. In Fig. 6, the left lateral ventricle (red arrow) of ANTs registered image shrinks. By comparison, the BD gives the best registration results. Such quantitative differences can be critical from the standpoint of clinical analysis, whenever ventricular shape differences and volume ratios between acute and chronic time points are of interest. Please refer to the following webpage for additional validation results: https://sites.google.com/site/louyifei/research/tbi

It is worth noticing that the topology changes around a hemorrhaging white matter region (blue arrow) in the FLAIR image of Fig. 6. The structure is ambiguous in the corresponding area of T_1 due to the inability of the latter technique to distinguish between edemic and nonedemic tissue, on the one hand, and between hemorrhagic and nonhemorrhagic edema, on the other hand. The FLAIR images as deformed by various registration methods have different visual features in Fig. 6. All these methods assume that the deformation field is smooth; when this assumption is not valid, each method imposes its own interpretation of the "correct" deformation. Though important, it is difficult to design registration algorithms which can handle topological changes, especially for registering TBI data across time. This is beyond the scope of this paper and will be our future research direction.

D. Clinical Significance

Robust methods for TBI assessment can play an essential role during both acute and chronic therapy of this condition for several reasons. First, it is well appreciated that proper management of TBI sequelae can alter their course, improve mortality and morbidity, reduce hospital stay, and decrease health care costs [42]. Consequently, TBI neuroimaging is important for surgical planning by providing useful information for guiding decisions concerning the aggressiveness of TBI treatment [2]. Nevertheless, the application of automatic MRI image processing algorithms to the clinical assessment of TBI cases remains problematic due to the fact that many existing methods are insufficiently robust from the standpoint of accurately capturing TBI-related changes in brain anatomy [43]–[45]. Thus, although significant recent progress has been achieved in the development of image analysis tools, TBI quantification remains difficult, particularly for the purpose of improving clinical outcome metrics.

In Fig. 7, the norms of the deformation fields and their 2-D motion grid are included for both the acute and chronic stages. For the T_2, FLAIR and GRE volumes, the largest amount of deformation is observed bilaterally in the deep periventricular white matter, possibly as a consequence of hemorrhage and/or CSF infiltration into edemic regions, which can alter voxel intensities in GRE and FLAIR imaging, respectively. In the case of DWI, notable deformation is observed frontally and frontolaterally; in the former case, this may be the result of warping

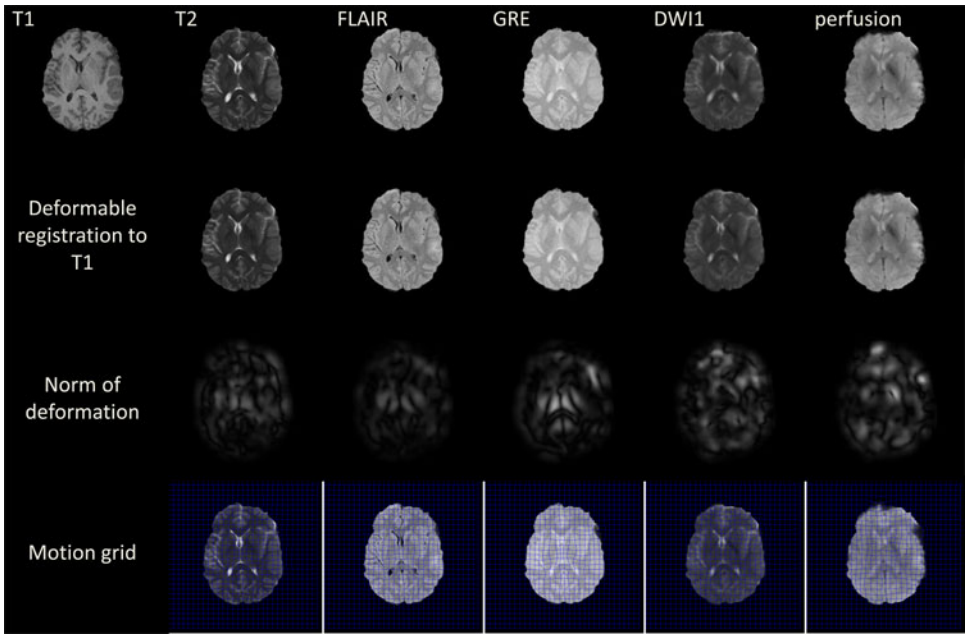

Fig. 7. Results of registering five volumes acquired at the acute time point (columns 2–6) to the acute T_1 volume (column 1).

artifacts due to the large drop in the physical properties of tissues at the interfaces between brain, bone, and air. In the latter case, the deformation is possibly due to the presence of TBI-related edema, which can substantially alter local diffusivity values. Similar effects due to these causes are observed with DWI and with perfusion imaging in both acute and chronic scans.

Our visual representations involving deformation norms and motion grids can be interpreted as error maps, which allow one to acquire improved understanding of how pathology discriminately affects each imaging modality. This may be useful in order to ascertain how various phenomena associated with TBI pathology (e.g., the deformation norm of CSF-perfused edema in the case of FLAIR or hemorrhage in the case of GRE imaging) can affect brain shape and tissues. For example, large deformation field norms associated with periventricular pathology at the acute time point (as obviated in Fig. 7) can be conceptualized as quantitative indicators regarding the spatial extent and manner in which aspects of the pathology captured by each of these techniques affect brain tissues differentially.

VI. Conclusion and Future Research

We have presented a new similarity measure based on the BD for multimodal image registration of TBI MR images. The measure was compared to the standard MI method in a viscous fluid framework. The performance of the two metrics was compared quantitatively and qualitatively using synthetic phantoms and simulated MRIs with artificial and known deformations. The proposed algorithm was implemented on the GPU and was found to take 6 sto register two MR volumes of typical matrix sizes. In addition to the ability to perform fast deformable registration of TBI volumes, the paradigm presented in this paper also introduces the use of deformation maps and motion grids as visualization tools with potential clinical application.

Future work will focus on the registration of TBI volumes across time [46]. There are a large number of registration algorithms which assume smoothness of the vector flow, i.e., that the deformation is diffeomorphic; however, when registering TBI volumes across time, the deformation is not often well defined, let alone diffeomorphic, in regions where hemorrhage or edema occur. Consequently, it is challenging though important to design registration algorithms which can accommodate topological changes occurring in TBI patients. There are a few studies working along this direction, such as [47] and [48]. The registration of longitudinal TBI is beyond the scope of this paper and will be our future work.

References

[1] M. Faul, L. Xu, M. Wald, and V. Coronado. (2010). Traumatic brain injury in the united states: Emergency department visits, hospitalizations and deaths 2002-2006. Atlanta, GA: Centers for Disease Control and Prevention, National Center for Injury Prevention and Control [Online]. Available:http://www.cdc.gov/traumaticbraininjury/pdf/bluebook.pdf

[2] R. M. Chesnut, "Implications of the guidelines for the management of severe head injury for the practicing neurosurgeon," *Surg. Neurol.*, vol. 50, pp. 187–193, 1998.

[3] W. M. Wells, P. Viola, H. Atsumid, S. Nakajimae, and R. Kikinise, "Multimodal volume registration by maximization of mutual information," *Med. Image Anal.*, vol. 1, no. 1, pp. 35–51, 1996.

[4] P. Viola and W. M. Wells, "Alignment by maximization of mutual information," *Int. J. Comput. Vis.*, vol. 24, pp. 137–154, Sep. 1997.

[5] F. Maes, A. Collignon, D. Vandermeulen, G. Marchal, and P. Suetens, "Multimodality image registration by maximization of mutual information," *IEEE Trans. Med. Imag.*, vol. 16, no. 2, pp. 187–198, Apr. 1997.

[6] J. P. W. Pluim, J. B. A. Maintz, and M. A. Viergever, "Mutual-information-based registration of medical images: A survey," *IEEE Trans. Med. Imag.*, vol. 22, no. 8, pp. 986–1004, Aug. 2003.

[7] Q. R. Razlighi, N. Kehtarnavaz, and A. Nosratinia, "Computation of image spatial entropy using quadrilateral markov random field," *IEEE Trans. Image Proc.*, vol. 18, no. 12, pp. 2629–2639, Dec. 2009.

[8] Z. Yi and S. Soatto, "Nonrigid registration combining global and local statistics," in *Proc. IEEE Conf. Comput. Vis. Pattern Recognit.*, Jun. 2009, pp. 2200–2207.

[9] D. Loeckx, P. Slagmolen, F. Maes, D. Vandermeulen, and P. Suetens, "Nonrigid image registration using conditional mutual information," *IEEE Trans. Med. Imag.*, vol. 29, no. 1, pp. 19–29, Jan. 2010.

[10] J. Chappelow, B. Bloch, N. Rofsky, E. Genega, R. Lenkinski, W. DeWolf, and A. Madabhushi, "Elastic registration of multimodal prostate MRI and histology via multiattribute combined mutual information," *Med. Phys.*, vol. 38, no. 4, pp. 2005–2018, 2011.

[11] S. Kullback and R. A. Leibler, "On information and sufficiency," *Ann. Math. Statist.*, vol. 22, no. 1, pp. 79–86, 1951.

[12] T. Leung and J. Malik, "Representing and recognizing the visual appearance of materials using three-dimensional textons," *Int. J. Comput. Vis.*, vol. 43, no. 1, pp. 29–44, 2001.

[13] A. Bhattacharyya, "On a measure of divergence between two statistical populations defined by their probability distributions," *Bull. Calcutta Math. Soc.*, vol. 35, pp. 99–109, 1943.

[14] M.-C. Chiang, R. A. Dutton, K. M. Hayashi, A. W. Toga, O. L. Lopez, H. Aizenstein, J. T. Becker, and P. M. Thompson, "Fluid registration of medical images using jensen-renyi divergence reveals 3d profile of brain atrophy in HIV/AIDS," in *Proc. Int. Symp. Biomed. Imag. (ISBI)*, 2006, pp. 193–196.

[15] J. P. W. Pluim, J. B. A. Maintz, and M. A. Viergever, "F-information measures in medical image registration," *IEEE Trans. Med. Imag.*, vol. 23, no. 12, pp. 1508–1516, Dec. 2004.

[16] F. Aherne, N. Thacker, and P. Rockett, "The Bhattacharyya metric as an absolute similarity measure for frequency coded data," *Kybernetika*, vol. 34, no. 4, pp. 363–368, 1997.

[17] T. Kailath, "The divergence and bhattacharyya distance measures in signal selection," *IEEE Trans. Commun. Technol.*, vol. COM-15, no. 1, pp. 52–60, Feb. 1967.

[18] F. Goudail, P. Refregier, and G. Delyon, "Bhattacharyya distance as a contrast parameter for statistical processing of noisy optical images," *J. Opt. Soc. Amer. A*, vol. 21, no. 7, pp. 1231–1240, 2004.

[19] O. Michailovich, Y. Rathi, and A. Tannenbaum, "Image segmentation using active contours driven by the bhattacharyya gradient flow," *IEEE Trans. Image Proc.*, vol. 16, no. 11, pp. 2787–2801, Nov. 2007.

[20] D. Freedman and T. Zhang, "Active contours for tracking distributions," *IEEE Trans. Image Proc.*, vol. 13, no. 4, pp. 518–526, Apr. 2004.

[21] I. R. Khan and F. Farbiz, "A new similarity measure and back-projection scheme for robust object tracking," in *Proc. IEEE Int. Symp. Commun. Inf. Technol.*, Oct. 2010, pp. 26–29.

[22] E. D'Agostino, F. Maes, D. Vandermeulen, and P. Suetens, "A viscous fluid model for multimodal non-rigid image registration using mutual information," in *Proc. Int. Conf. Med. Image Comput. Comput.-Assist. Intervent.-Part II ser. MICCAI*, 2002, pp. 541–548.

[23] D. Rueckert, L. I. Sonoda, C. Hayes, D. L. G. Hill, M. O. Leach, and D. J. Hawkes, "Nonrigid registration using free-form deformations: Application to breast MR images," *IEEE Trans. Med. Imag.*, vol. 18, no. 8, pp. 712–721, Aug. 1999.

[24] G. E. Christensen, R. D. Rabbitt, and M. I. Miller, "Deformable templates using large deformation kinetics," *IEEE Trans. Image Proc.*, vol. 5, no. 10, pp. 1435–1447, Oct. 1996.

[25] N. D. Cahill, J. A. Noble, and D. J. Hawkes, "Fourier methods for nonparametric image registration," in *Proc. IEEE Conf. Comput. Vis. Pattern Recognit.*, Jun. 2007, pp. 1–8.

[26] M. Bro-Nielsen and C. Gramkow, "Fast fluid registration of medical images," in *Proc. 4th Int. Conf. Vis. Biomed. Comput.*, 1996, pp. 267–276.

[27] F. Beg, M. Miller, A. Trouve, and L. Younes, "Computing large deformation metric mappings via geodesic flows of diffeomorphisms," *Int. J. Comput. Vis.*, vol. 61, no. 2, pp. 139–157, Feb. 2005.

[28] L. Younes, F. Arrate, and M. Miller, "Evolutions equations in computational anatomy," *Neuroimage*, vol. 45, pp. S40–50, Mar. 2009.

[29] M. Niethammer, Y. Huang, and F. X. Vialard, "Geodesic regression for image time-series," in *Proc. Med. Image Comput. Comput.-Assist. Intervent. (MICCAI)*, 2011, vol. 6892, pp. 655–662.

[30] Y. Lou, X. Jia, X. Gu, and A. Tannenbaum. (2011, May). A GPU-based implementation of multimodal deformable image registration based on mutual information or Bhattacharyya distance. *Insight J.* [Online]. Available:http://www.midasjournal.org/browse/publication/803/

[31] D. Collins, A. Zijdenbos, V. Kollokian, J. Sled, N. Kabani, C. Holmes, and A. Evans, "Design and construction of a realistic digital brain phantom," *IEEE Trans. Med. Imag.*, vol. 17, no. 3, pp. 463–468, Jun. 1998.

[32] D. Skerl, B. Likar, and F. Pernus, "A protocol for evaluation of similarity measure for non-rigid registration," *Med. Image Anal.*, vol. 12, no. 1, pp. 42–54, Feb. 2008.

[33] J. Mugler and J. Brookeman, "Three-dimensional magnetization-prepared rapid gradient-echo imaging (3D MP RAGE)," *Magn. Reson. Med.*, vol. 15, pp. 152–157, 1990.

[34] B. De Coene, J. Hajnal, P. Gatehouse, D. Longmore, S. White, J. Oatridge, A. Pennock, I. Young, and G. Bydder, "MR of the brain using fluid-attenuated inversion recovery (FLAIR) pulse sequences," *AJNR Amer. J. Neuroradiol.*, vol. 13, no. 6, pp. 1555–1564, 1992.

[35] S. Huh, T. A. Ketter, K. H. Sohn, and C. Lee, "Automated cerebrum segmentation from three-dimensional sagittal brain MR images," *Comput. Biol. Med.*, vol. 32, pp. 311–328, 2002.

[36] A. H. Zhuang, D. J. Valentino, and A. W. Toga, "Skull-stripping magnetic resonance brain images using a model-based level set," *NeuroImage*, vol. 32, pp. 79–92, 2006.

[37] J. Acosta-Cabronero, G. B. Williams, J. M. Pereira, G. Pengas, and P. J. Nestor, "The impact of skull-stripping and radio-frequency bias correction on grey-matter segmentation for voxel-based morphometry," *NeuroImage*, vol. 39, pp. 1654–1665, 2008.

[38] D. W. Shattuck and R. M. Leahy. (2002). BrainSuite: An automated cortical surface identification tool. *Med. Image Anal.* [Online]. *8(2)*, pp. 129–142. Available: http://users.loni.ucla.edu/shattuck/brainsuite/corticalsurface/bse/

[39] H. Johnson, G. Harris, and K. Williams. (2007). BRAINSFit: Mutual information registrations of whole-brain 3D images, using the insight toolkit. [Online]. Available:http://hdl.handle.net/1926/1291

[40] M. Modat, G. R. Ridgway, Z. A. Taylor, M. Lehmann, J. Barnes, D. J. Hawkes, N. C. Fox, and S. Ourselin, "Fast free-form deformation using graphics processing units," *Comput. Methods Progr. Biomed.*, vol. 98, no. 3, pp. 278–284, 2010.

[41] B. B. Avants, C. L. Epstein, M. Grossman, and J. C. Gee, "Symmetric diffeomorphic image registration with cross-correlation: Evaluating automated labeling of elderly and neurodegenerative brain," *Med. Image Anal.*, vol. 12, pp. 26–41, 2008.

[42] D. Watts, M. Hanfling, D. Waller, C. Gilmore, S. Fakhry, and A. Trask, "An evaluation of the use of guidelines in prehospital management of brain injury," *Prehosp. Emerg. Care*, vol. 8, pp. 254–261, 2004.

[43] A. Irimia, M. C. Chambers, J. R. Alger, M. Filippou, M. W. Prastawa, B. Wang, D. A. Hovda, G. Gerig, A. W. Toga, R. Kikinis, P. M. Vespa, and J. D. Van Horn, "Comparison of acute and chronic traumatic brain injury using semi-automatic multimodal segmentation of MR volumes," *J. Neurotrauma*, vol. 28, pp. 1–20, 2011.

[44] A. Irimia, M. C. Chambers, C. M. Torgerson, M. Filippou, D. A. Hovda, J. R. Alger, G. Gerig, A. W. Toga, P. M. Vespa, R. Kikinis, and J. D. Van Horn, "Patient-tailored connectomics visualization for the assessment of white matter atrophy in traumatic brain injury," *Front. Neurol.*, vol. 3, no. 1, pp. 1–21, 2012.

[45] A. Irimia, B. Wang, S. R. Aylward, M. W. Prastawa, D. F. Pace, G. Gerig, D. A. Hovda, R. Kikinis, P. M. Vespa, and J. D. Van Horn, "Neuroimaging of structural pathology and connectomics in traumatic brain injury: Toward personalized outcome prediction," *NeuroImage: Clin.*, vol. 1, pp. 1–17, 2012.

[46] B. Wang, M. Prastawa, A. Irimia, M. C. Chambers, P. M. Vespa, J. D. Van Horn, and G. Gerig, "A patient-specific segmentation framework for longitudinal MR images of traumatic brain injury," in *Proc. SPIE Med. Imag.*, 2012, vol. 8413, pp. 841302-1–841302-7.

[47] M. Niethammer, G. Hart, D. Pace, and S. Aylward, "Geometric metamorphosis," in *Proc. MICCAI*, 2011, pp. 639–646.

[48] B. Wang, M. Prastawa, S. P. Awate, A. Irimia, M. C. Chambers, P. M. Vespa, J. D. Van Horn, and G. Gerig, "Segmentation of serial MRI of TBI patients using personalized atlas construction and topological change estimation," in *Proc. IEEE Int. Symp. Biomed. Imag. (ISBI)*, 2012, pp. 1152–1155.

Authors' photographs and biographies not available at the time of publication.